Effects of CDS and drying temperature on the flowability behavior of DDGS

Rumela Bhadra, K. Muthukumarappan, Kurt A. Rosentrater

Published Version Information

Citation: Bhadra, R., Muthukumarappan, K., & Rosentrater, K. A. (2012). Effects of CDS and drying temperature on the flowability behavior of DDGS. Drying Technology: An International Journal, 30(5), 542-558.

Digital Object Identifier (DOI): doi:10.1080/07373937.2011.649510

Publisher's Link: http://www.tandfonline.com/doi/abs/10.1080/07373937.2011.649510

TITLE: EFFECTS OF CDS AND DRYING TEMPERATURE LEVELS ON THE FLOWABILITY BEHAVIOR OF DDGS

Author(s)

Rumela Bhadra, PhD, Post-Doctoral Research Associate, BAE Department, Kansas State University, Manhattan, Kansas. **Email:** rumelabhadra31@yahoo.com

Address: 147 Seaton Hall, BAE Department, Kansas State University, Manhattan, KS 66502

K. Muthukumarappan, PhD, Professor, Department of Agricultural and Biosystems Engineering, South Dakota State University, South Dakota. **Email:** muthukum@sdstate.edu

Address: 1400 North Campus Drive, South Dakota State University, Brookings, SD 57007

Kurt A. Rosentrater, PhD, Assistant Professor, Department of Agricultural and Biosystems Engineering, Iowa State University, IA. **Email:** karosent@iastate.edu

Address: Iowa State University, Department of Agricultural and Biosystems Engineering, 3167 NSRIC Building, Ames, IA 50011

Corresponding author: Kurt A. Rosentrater, PhD, Assistant Professor, **Address:** Iowa State University, Department of Agricultural and Biosystems Engineering, 3167 NSRIC Building, Ames, IA 50011. **Email:** karosent@iastate.edu

Phone: (515) 294-4019; **Fax:** (515) 294-6633

ABSTRACT

Due to increasing demand for alternative fuels and the need to reduce dependence on fossil fuels, the growth of bioethanol production has been rising. One of the problems facing this industry is transportation of the coproduct distillers dried grains with solubles (DDGS) over long distances, because caking and agglomeration between particles can lead to bulk flow problems. In this study DDGS was prepared by combining condensed distillers solubles (CDS) and distillers wet grains (DWG), and then oven drying to achieve 8% (db) moisture content. The effects of drying temperature (100, 200, and 300ºC) and CDS (10, 15, and 20% wb) level on the resulting flowability behavior of the DDGS particles were investigated. Statistical analyses indicated significant differences ($\alpha = 0.05$, 95% confidence level) due to drying temperature and CDS main effects, and also significant interaction effects between CDS level and drying temperature for many of the flow parameters. Surface regression analysis of the ratio of Total Flow Index/Jenike Flow Function as a function of CDS and drying temperature resulted in an R^2 value of 0.94. Partial Least Squares (PLS) regression yielded an R^2 of 0.90 for the Jenike Flow Function Index as a function of all flow and physical properties, using only two multivariate components. Understanding the effects of varying drying temperature and CDS levels can help guide efforts to overcome DDGS flowability problems.

Keywords. Agglomeration, Caking, Carr, Condensed distillers solubles, Distillers wet grains, Jenike.

INTRODUCTION

Distillers dried grains with solubles (DDGS) is a coproduct from the corn-based fuel ethanol industry, and is relatively high in protein and fiber content but low in starch. Due to its nutrient content and digestibility, it is primarily used as livestock feed for beef and dairy rations, and to some extent in swine and poultry diets. Research has also been done on using DDGS in aquaculture feed (1) As there is growing demand for fuel ethanol, there is more production of DDGS as well. It has been reported that during the fiscal year of 2008-2009, over 19 million metric tons of DDGS was produced from the ethanol industry in United States (2), and this level has risen to more than 30 million metric tons in 2010.

In order to optimize the use of DDGS in livestock feed markets, it is therefore essential to provide safe and economic handling of DDGS while it is being transported in domestic as well as international markets. Distillers dried grains with solubles storage and transportation is often problematic due to formation of particle agglomerates inside storage structures, which results in "caking" and restricts flow during discharge. Flowability problems may be due to varied environmental conditions and storage situations, such as temperature, moisture content, humidity, and storage period. Apart from environmental conditions, the inherent physical and chemical properties of the material may also affect overall flowability of DDGS (3; 4; 5). Cohesiveness and flow problems create unwanted labor and cost to unload (6).

Most organic materials (like DDGS) are hygroscopic in nature, so they have the tendency to gain or lose moisture when they are exposed to diverse humidity conditions. This can lead to possible changes in physical and chemical properties in the material itself, which in turn will affect the flowability and can cause hardening of particles.

Condensed Distillers Solubles (CDS), commonly known as “solubles” or “syrup,” is mixed with distillers wet grains (DWG) and then dried to produce distillers dried grains with solubles (DDGS). The solubles are relatively high in vitamins, fat (6-21%, db), and protein (9-12%, db), but low in fiber (<5%, db). Syrup has a total digestible energy value approximately 91% that of raw corn (7). DDGS typically contains approximately 86 to 93% dry matter, 3 to 13% (db) fat, and 26 to 34% (db) protein (8). The high fat level in CDS may be a possible cause for DDGS flowability problems, because the corn lipids may form molten bridges between the particles

Stickiness in corn syrup powders was determined under varying temperature and humidity conditions (9). The effect of temperature, moisture content, and storage time was studied for milk powder flowability and stickiness (10; 11; 12). It has been found that powder caking is often a function of moisture content, and frequently there is an increase in stickiness due to an increase in ambient temperature (13; 14).

Powder flowability is most commonly assessed using Carr (15) and Jenike (16) shear test procedures. Parameters for flowability in the Carr (15) test procedure include Angle of Repose (AoR), Aerated and Packed Bulk Density (ABD and PBD), Compressibility (Cc), Angle of Spatula (AoS), Angle of Difference (AoD), Uniformity, Angle of Fall (AoF), Dispersibility, and Total Flow and Flood Indices. Hausner Ratio is defined as the ratio of tapped bulk density to the aerated (or apparent) bulk density (i.e., PBD/ABD). Values less than 1.25 typically indicate good flow, whereas values greater than 1.25 generally indicate poor flow (17). Angle of Spatula is measured by inserting a flat blade into a pile of powder and then lifting it up. After the evaluation of the above properties (i.e., Angle of Repose through Uniformity) (excluding Hausner Ratio), the index values are combined to provide an overall flowability index value for the powder/bulk solid under investigation. The smaller the uniformity value, the more homogenous the particle shapes are, and typically the less the flow problem (15, 17).

After the overall (or total) flowability index has been determined, then the floodability assessment is done. The Angle of Fall, the Angle of Difference, and Dispersibility is measured as part of floodability index. The above properties (Angle of Fall, Angle of Difference, and Dispersibility, in addition to Flow Index) are numerically combined to calculate the Total Floodability Index of the bulk solid (by summation of the individual indices). The angle of fall is the new angle of repose that is formed after impaction has been applied to the material. More detailed information on these properties and testing procedures can be found in Carr (15) and Bhadra et al. (3).

Another procedure which is used commonly to assess flow behavior is Jenike (16) shear testing. In this type of test, when the powder is subjected to a normal stress (σ), there will be a particular shear stress (τ) which causes bulk failure (i.e., flow). This data gives the yield locus curve which can be used to compute the angle of internal friction (Φ, degrees), effective angle of internal friction (δ, degrees), major consolidation stress (σ_1, kPa), and unconfined yield strength (σ_c, kPa).

Unconfined yield strength is a measure of the compressive strength (kPa) of the granular solid (18). Major consolidation stress is determined as the point of intersection between the Mohr circle (drawn with a shear and normal stress plot) and the stress x-axis. Flow Function Index (dimensionless) is the ratio of the major consolidation stress to unconfined yield strength. Depending on the value of this index, the flow behavior of a material can be categorized as "good flow", "fair to passable flow," or "cohesive flow." More details on this can be found in Jenike (16) and Bhadra et al. (3).

Some work has previously examined DDGS flowability, including use of flow agents, measuring physical and chemical properties and correlating them with the Carr and Jenike shear test properties (19; 20; 21; 22). Reduced fat and normal DDGS samples have been studied to understand flow properties, and reduced fat DDGS had slightly better flow that normal DDGS (5). Previous work has also shown the effects of moisture content and CDS addition levels on DDGS flowability (19). Development of a predictive flowability model ($R^2 = 0.94$) using exploratory data analysis techniques was accomplished (21). A comprehensive dynamic water adsorption model (GRM model, $R^2 = 0.94$) incorporating varying CDS, relative humidity, and drying temperature levels has been developed (22). A model ($R^2 = 0.94$) to predict the sorption isotherm behavior of DDGS with varying CDS and equilibrium moisture content levels was also developed (23). Various studies have also revealed the typical ranges of DDGS chemical, physical, and flowability properties (3; 4; 24).

The functionality and properties of bulk solids and granular materials are greatly influenced by drying conditions during the manufacturing process (46, 47, 48, 49). Two studies examined drying rate and moisture desorption during DDGS production, using varying CDS and drying temperature levels (25; 26). Those studies were able to establish regression models of the drying kinetics and moisture desorption behavior; but no correlational studies between the resulting flowability properties and the effects of drying temperature and CDS addition levels were performed. Understanding these effects on physical and flow properties is an essential step toward improving DDGS flowability.

Therefore, the objectives of this study were: 1) to prepare DDGS samples under laboratory conditions using CDS and DWG using multiple ratios of CDS:DWG and multiple drying temperatures; 2) to measure several physical and flow properties (both Carr and Jenike flow properties) of the prepared DDGS samples; 3) to determine the effects of drying temperature and CDS addition levels on the resulting properties of the DDGS; and 4) to examine predictive regression models of various DDGS properties to fully understand the effects CDS level and drying temperature.

MATERIALS AND METHODS

Sample Collection and Preparation

Samples of distillers wet grains (DWG) and condensed distillers solubles (CDS) were collected from a commercial fuel ethanol plant in South Dakota and were stored under refrigerated conditions (10 ± 1°C). The initial moisture content of the DWG and CDS samples were between 45% (db) to 47% (db). Prior to the drying experiments, CDS was added to DWG at several predetermined levels (10, 15, and 20%, wb), and then thoroughly mixed in a laboratory mixer (model D300, Hobart Corporation, Troy, OH) for 5 min. After blending, each combined sample (approximately 350 g of mixed DWG and CDS) was spread uniformly on a thin aluminum plate (38 cm × 27 cm × 2 cm) and then dried in a laboratory-scale oven (model 838F, Fisher Scientific, Pittsburg, PA). For a single drying temperature and CDS combination, three aluminum trays were used. Drying was done at three selected temperatures (100, 200, and 300°C) for each DWG/CDS mixture. Temperature selection was based on interviews and discussions with industry experts, and also based on our previous studies of drying rate and moisture content of DDGS (25; 26). For each temperature/CDS combination, drying was done to reduce all the experimental samples to a target of 8% (db) moisture content, in order to have common baseline moisture content and eliminate its possible influence on the flowability behavior. To achieve this, each treatment combination was dried at different drying times. The drying time slightly varied while changing the CDS levels: it was around 60 min, 35 min, and 15 min for drying temperatures of 100, 200, and 300°C, respectively. The drying continued until the final blend moisture contents reached 8% (db). This target was based on previous research by Bhadra et al. (24) and Rosentrater (27), and upon discussions with industry representatives (unpublished), which indicated a typical average moisture content of approximately 8 % (db) in the marketplace. Preparation of the dried DDGS samples (9 total treatments) was done with three replications.

Experimental Design

Experiments were conducted using a 3*3 full factorial design, with 3 drying temperatures (100, 200, and 300°C) and 3 CDS addition levels (10, 15, and 20%, wb), yielding a total of 9 treatment combinations. These treatment combinations were implemented using a completely randomized design. DDGS samples were prepared in three replications, thus yielding 3*3*3 = 27 experimental runs. Each physical and flow property was determined using three replicate measurements for each treatment combination.

Once the drying was completed, the granular particles of each sample were cooled for 6 to 8 h under ambient conditions (~25^{o}C), and then placed in polyethylene bags and stored at room temperature (~25^{o}C), throughout the duration of the study. After the drying was completed for all 27 experimental runs, the physical and flow properties were then measured.

Flowability Property Measurement

A powder characteristics tester (Model PTR, Hosokawa Micron Powder Systems, Summit, NJ) was used to measure the Carr (15) flow properties of the DDGS, following the procedures described by ASTM D6393 (28). The Carr flow properties included AoR, ABD, PBD, Compressibility, Uniformity, AoF, AoS, AoD, and Dispersibility. These parameters were then used to determine both the Total Flow Index and Total Floodability Index.

AoR is defined as the angle formed between the slope of a pile of material and a horizontal plane. ABD and PBD are used to assess compressibility and the ability of the material to entrap air in pores between particles (29). Packed (or tapped) density is an actual representation of a material's bulk density when it is stored in bins or transported over large distances (i.e., in a rail car as entrained air is forced out). Angle of Spatula is measured by inserting a flat blade into a pile of material and then lifting it up. The new Angle of Repose which the material forms relative to the horizontal plane of the blade gives the Angle of Spatula. Uniformity is the ratio of the width of the sieve opening that will allow 60% of the material to pass to the width of sieve opening that will only allow 10% of the sample to pass. Uniformity thus gives a relative measure of the homogeneity of the size and shape of the particles. Uniformity is the ratio obtained between the width of sieve opening that will pass 60% of the sample to the width of sieve opening that will pass only 10% of the sample. Particle size distributions were determined using standard US sieves, from no. 4 (pore opening size of 4.76 mm) to 270 (pore opening size of 53 μm). Thus, the Total Flow Index was determined by adding the Angle of Repose, Uniformity, Compressibility, and Angle of Spatula.

After the overall flowability index has been determined, then floodability is assessed. The Angle of Fall is the new angle of repose that is formed after impaction (by the impactor device provided on the Hosokawa Micron Powder System Unit) has been applied to the material. It is done to simulate the disturbance due to vibrations and transport effects on bulk solids (15). . The Angle of Difference is then calculated by subtracting the Angle of Fall from the Angle of Repose. Dispersibility is measured by discharging a specified amount (10 g) of material through a column onto a watch glass 98 cm diameter); the quantity of material left behind on the watch glass quantifies how disperse the material is. Hence, Total Floodability Index was determined by adding the Angle of Fall, Angle of Difference, Dispersibility, and Total Flow Index.

The other flowability behavior is measured by Jenike (16) shear testing. This method uses a split, horizontal testing container, and various normal stresses and shear stresses are applied to the top half, while the lower half is kept stationary. In this type of test, when the powder is subjected to a normal stress (σ), there will be a particular shear stress (τ) which causes bulk failure (i.e., flow). This data gives the yield locus curve, which can then be used to compute the angle of internal friction (Φ, degrees), effective angle of internal friction (δ, degrees), major consolidation stress (σ_1, kPa), and unconfined yield strength ($\sigma_{c,}$ kPa). Angle of internal friction is the inter-particle friction as the bulk solid tends to slide on itself at the onset of flow. Effective angle of internal friction is measured during flow when granular solids are constantly exposed to pressures. The major pressure acting on a particle element is denoted by σ_1 while the minor pressure is termed σ_2. The relationship between these two pressures varies slightly with changes in temperature for most bulk solids (1964). Their relationship can be expressed as:

$$\frac{\sigma_1}{\sigma_2} = \frac{1+\sin\delta}{1-\sin\delta} \qquad (1)$$

This equation is called the effective yield function. It describes inter-particle kinematic particle friction which exists during steady flow. Unconfined yield strength is a measure of the compressive strength (kPa) of the granular solid (18). Major consolidation stress is determined as the point of intersection between the Mohr circle and the stress x-axis. Major consolidation stress

(σ_1, kPa) was calculated from the Mohr circles, which are drawn from the equation of effective yield function (i.e., equation 1). The point where the largest Mohr circle intersects the normal stress axis (i.e., x-axis) gives σ_1. Additionally, σ_c (unconfined yield strength, kPa) was determined from the Mohr circle as well. It is the intersection of the smaller Mohr circle on the normal stress axis. Flow Function Index (dimensionless) is the ratio of the major consolidation stress (σ_1, kPa) to unconfined yield strength (σ_c, kPa).

Jenike (16) shear testing was then performed to quantify the instantaneous shear behavior for each DDGS sample, including angle of internal friction, effective angle of internal friction, major consolidation stress, unconfined yield strength, and Jenike Flow Index. A Jenike shear cell unit was used (Model ST-5, Jenike and Johansson Co., Westford, MA) following the procedures described in ASTM D6128 (30). Jenike compressibility testing was also performed using the same shear cell unit, but using the technique discussed in ASTM D6683 (31).

Physical Property Measurement

Color and thermal properties are not directly correlated with flowability properties of DDGS however, there can some indirect effects. For example, color and brightness of a product can indicate the level of nutrients (carbohydrates, lipids, fiber, etc.), which can, in turn, affect the flow properties of DDGS. Similarly, thermal properties can correlate to frictional properties, which, in turn, affect flow behavior. Water activity changes can indicate shelf life. PDI provides a measure of protein solubility, which interacts with surface moisture films between DDGS particles.

Color was measured using a spectrophotocolorimeter (LabScan XE, Hunter Associates Laboratory, Reston, VA) with the L-a-b color scale (Hunter Associates Laboratory Universal Software Manual V. 2.5; Reston; VA). Water activity was measured using a calibrated water activity meter (AW Sprint TH 500, Novasina, Talstrasse, Switzerland) using factory-supplied standards. Thermal properties (conductivity, diffusivity, and resistivity) were determined with a thermal properties meter (KD2, Decagon Devices, Pullman, WA) that utilized the line heat source probe technique (32). Geometric mean diameter (GMD) (average particle size) was determined by ASAE standard method S319.3 (33) with a Rotap sieve shaker (model RX-29, Tyler Manufacturing, Mentor, OH). Porosity of the DDGS samples was calculated from the method described in Sahin and Sumnu (34) using a multivolume pycnometer (model 1305, Micromeritics, Norcross, GA). The protein dispersibility index (PDI) was calculated using AACC method 46-24 (35).

Statistical Analysis

Formal statistical data analyses were performed using Microsoft Excel v.2003 (Microsoft Corp., Redmond, WA) and SAS v.8 (SAS Institute, Cary, NC) software. Analyses included summary statistics, analysis of variance (at $\alpha = 0.05$), and Least Significant Difference (LSD) (at $\alpha = 0.05$) testing; these were performed to determine significant differences and interaction effects between the main effects and treatment combination effects due to drying temperature and CDS level. Pearson linear correlation analysis among all properties was performed to examine relationships at the 95% confidence level. TableCurve 3D v.4.0.01 (SYSTAT Software, Inc., San Jose, CA) was then used to develop regression equations and response surface models. Partial Least Squares (PLS) and Principal Component Analysis (PCA) tests were then performed using Minitab v.14 software (Minitab, State College, PA).

RESULTS AND DISCUSSION

Main Effects, Interaction Effects and Treatment Combination Effects

Table 1 gives the summary of the statistical output obtained after examining main effects on all of the physical and flow properties. It was observed that there were significant differences in the main effects for both CDS addition and drying temperature levels using the Least Significant (LSD) test. To verify these differences, Tukey's significance test (TSD) at $\alpha = 0.05$ was also performed, and similar significant differences (although they are not reported here) was observed (36). Even for a conservative test like TSD, significant differences were observed for most of the physical and flowability properties. Flowability of DDGS is a multivariate phenomenon, as reflected by these results. Considerable variability in physical and flowability properties was also found in commercial DDGS samples collected from various ethanol plants (27).

These results also verify our hypothesis that drying temperature and CDS level results in significant differences in DDGS properties. For example, there was a significant increase in geometric mean diameter when drying temperature increased from 200 (0.78 mm) to 300°C (0.99 mm). Even though the DDGS moisture content was constant for all the samples produced (8% db, as stated earlier), higher drying temperatures produced larger particle sizes. Large particle sizes generally result in decreased flow problems in bulk solids. Increasing CDS levels from 10% (0.91 mm) to 15% (0.75 mm) resulted in a significant decrease in particle size, indicating possible flow problems. However, geometric mean diameter showed an interaction effect between CDS and temperature. CDS*temperature increased the particle size overall (0.67 to 1.31 mm), except at 300°C (from 15 and 20% CDS), where particle size was slightly reduced to 0.81 mm. Angle of Repose increased (42.06° to 47.16°) with increased CDS*temperature combinations; higher angles indicate poorer flow. For water activity, CDS*temperature led to a decrease in value (from 0.71 to 0.23) as the temperature was increased. More details of CDS*temperature interaction effects are discussed in later sections.

As shown in Table 2, there were also significant interaction effects ($p<0.05$) for varying CDS levels and drying temperatures for most of the physical and flowability properties, except for Hausner Ratio (HR, -) and Carr Compressibility (%).

There were significant differences among treatment combinations (Table 3) observed for most of trials. For a drying temperature of 100ºC, HR, PDI, and Carr Compressibility did not show any significant differences among the CDS levels (as indicated in bold letters). For a drying temperature of 200ºC, HR, AoF, Hunter L (-) (which measures the brightness or luminosity of a product), and thermal conductivity did not show significant differences among the CDS levels. For drying temperature of 300ºC, HR, Carr compressibility, Total Flow Index, angle of internal friction, major consolidation stress, Hunter a(-) (which refers to the redness or greenness of a product), and thermal conductivity did not shown any significant differences among the CDS levels. Thus, it can be concluded that at lower drying temperatures, changes in CDS levels can result in more variability in DDGS properties (both flow and physical) , which could lead to potential flow problems (3).

Property Relationships

Pearson product moment linear correlation analysis (37) was performed for the properties in this study (Table 4). The correlation coefficient quantifies how closely two properties are related to each other by a linear relationship. Only 19 combinations had p values less than $\alpha = 0.05$ (i.e., were significant correlations) and had correlation coefficient (r) values greater than 0.65. Out of these 19 combinations, 10 combinations had r values from |0.7| to |0.8|; 7 variable combinations had correlation coefficients from |0.8| to |0.9|; 2 combinations had r values from

|0.9| to |1.0|. A closer examination provides several insights. HR had a high correlation with Carr compressibility (C_c), which was anticipated because HR is calculated using PBD and ABD, which are basically the same parameters that are used to calculate C_c. Angle of Repose, an important parameter for flowability assessment, showed moderate correlation with uniformity; AoR is strongly dependent on the particle size and shape, and uniformity is measured via particle size. Higher drying temperature will cause the moisture to evaporate more effectively, thereby yielding lower water activity values, and hence improving the shelf life of the biomaterial. However, higher drying temperatures can increase utility costs in bioethanol plants.

Drying temperature was found to correlate with most of the properties. These tie in to our previous studies (25, 26) where mathematical modeling based on the same drying temperatures and CDS levels were used. In these studies, it was found that temperature had more significant effects on the drying behavior than CDS addition levels. It thus appears that drying temperature is mainly responsible for differences in physical and flow properties as well.

Effect of Drying Temperature and CDS Levels on Hausner Ratio (HR)

Hausner Ratio (-) values ranged from 1.05 to 1.25, depending on the drying temperature and CDS level (Figure 1). HR depends on the friction in a moving powder mass (i.e., internal friction) during the compaction of powders (38). Higher HR (>1.25) generally indicates poor flowability. In this study, the HR values were mostly below 1.25. As the drying temperature increased from 100 to 300ºC, the HR values decreased, indicating that higher temperatures yielded better DDGS flowability, for all CDS levels. For the 10% CDS level, the R^2 value (0.16) obtained from the regression equation was much less than other two CDS levels, which was probably due to the fact that there was substantial scatter in the data points at 100 and 300ºC. More extensive study with greater replications may provide a better regression equation.

However, for all CDS levels, the HR (-) decreased linearly with an increase in drying temperature, indicating better flow DDGS behavior.

Effect of Drying Temperature and CDS Levels on Jenike Flow Index

Figure 2 presents the flowability behavior of the DDGS samples based on Jenike Flow Index (16). In these flow functions, lines lying towards the bottom of the graph represent easy flow, while more difficult flow is indicated by lines lying near the top and the left of the graph; flowability worsens as the flow function moves upwards in an anticlockwise direction (5). At lower CDS levels (10%, wb), for 100ºC, the flow function line lies near the shear stress axis (y-axis), but for 200ºC and 300ºC, it moves towards the normal stress axis (x-axis). This indicates that DDGS with 10% CDS level and dried at 100ºC had a higher compressive strength, and thus greater ability to obstruct flow (i.e., was least free flowing). But higher drying temperatures (200 and 300°C) yielded better flowing DDGS with the same CDS level (10%, wb). For higher CDS levels (15 and 20%, wb), a shift in the flow function line towards the x-axis was observed, indicating better flowability, especially for the 200ºC and 300ºC drying temperatures. Generally, higher CDS levels will result in higher fat content among the DDGS particles, which may hinder flow, by forming bridges (i.e., molten or solidified fat layers) between particles, depending upon temperature. In this study, there were slight shifts of the flow function lines towards the x-axis, indicating better flow instead of flow obstruction. In some instances it has been found that higher CDS levels in DDGS may lubricate the materials and create easy flow (5). For all 3 CDS levels, the drying temperature showed similar behavior; higher temperature yielded better Jenike Flow Function Index line mostly inclined to x-axis, indicating good flow.

Effect of Drying Temperature and CDS Levels on Particle Size and Bulk Density

Figure 3 shows the effect of drying temperature on particle size and aerated bulk density of the DDGS samples for different CDS addition levels. With an increase in the drying temperature from 100 to 300ºC the bulk density slightly increased as did particle size, except for 20% (wb) CDS, where a decrease in the particle size from 100 to 200ºC was observed. There were also significant interactions between drying temperature and CDS (Table 3), thus the trend observed in particle size is not solely due to the main effect of drying temperature alone, but CDS and drying temperature together. These changes in particle size (due to the rapid formation of dried layers on the particle surfaces) with drying temperature were similar to findings by Chegini and Ghobadian (39). The particle size increase could be due to case hardening of the droplets at the higher temperatures, which leads to the formation of vapor–impermeable films on the drop surface, followed by the formation of vapor bubbles, and consequently droplet expansion. This hardened skin does not allow the moisture to exit from the droplet, and as a consequence the particle size is increases (39).

In terms of flowability, particle size plays an important role in the compressibility of powders. An increase in the particle size can lead to a reduction in the bulk density of the material, due to more entrapped void spaces (40) but for our samples, the bulk density slightly increased. This is may be due to the fact that increase in the particle size increased the mass of the solid, which was due to CDS. Thus, the overall bulk density increased. Lower particle sizes yield greater cohesive strength due to an increase in the surface/volume ratio between the particles (41). Thus, again from the particle size and bulk density perspective, similar results: the flowability was better with an increase in the drying temperatures at each CDS level, was noticed.

Effect of Drying Temperature and CDS Levels on Protein Dispersibility Index (PDI)

Protein Dispersibility Index estimates of the amount of water-soluble protein present in the sample. From Figure 4, a decrease in the PDI with an increase in the drying temperature for each CDS level was observed. Regression equations with R^2 values from 0.70 to 0.79 were obtained for all treatment combinations. Similar results of a decrease in PDI with an increase in processing temperature were obtained by Thomas et al., (42) and Qin et al., (43). In Thomas et al., (42) the decrease in PDI was linear with an increase in temperature for soy grits, similar to what was found in DDGS. But for Qin et al., (43) the decrease in PDI was exponential for full-fat soybeans collected from different origins. The decrease in PDI is due to the fact that at higher temperatures, the denaturation of protein occurs, and hence it changes the protein's biochemical and solubility properties. It was observed that heat processed soy flour had lower PDI values, but high nutritional content, and high consumption and marketability (44).

With respect to DDGS flowability problems, water soluble protein side chains may facilitate the formation of hydrogen bonds with the associated moisture film present between the particles, thus facilitating liquid bridging among particles. Increasing the drying temperature led to greater denaturing of the protein, which in turn reduced the water-soluble side chains and hence lowered PDI. But from a flowability perspective, lower PDI may mean a lower propensity to form liquid bridges, and hence, less particle caking..

Effect of Drying Temperature and CDS Levels on Flowability Indicator (ζ)

Figure 5 indicates the relationships between drying temperature and CDS addition levels with the "flowability indicator" parameter, ζ. This parameter was developed by Ganesan et al. (5), who established a predictive model for DDGS flowability based on combining Jenike and Carr data using Exploratory Data Analysis techniques:

$$\zeta = f\,(\text{Hausner Ratio}) \tag{2}$$

or

$$\zeta = \frac{Cc}{Dispersibility} \times \frac{\delta}{\Phi} \tag{3}$$

Where, C_c represents Carr compressibility, δ represents the effective angle of friction, and Φ represents the angle of internal friction. Generally, it has been found that lower regions in a flowability indicator plot indicate good flow. In Ganesan et al., (5) the flowability indicator plot for varying CDS and moisture contents resulted in a power law fit of $R^2 = 0.94$. For this study, higher drying temperature treatments occupied a position towards the origin of the plot, indicating better flow for those treatments. For 15% (wb) CDS addition levels, an R^2 value of 0.90 was obtained, but for 10% and 20% CDS levels, high R^2 values were not observed with a power law regression model. Similar results were obtained when fitting exponential regression equations to the data set, as indicated in Figure 6. Overall, the lower the drying temperature, the worse the DDGS flowability.

Regression Modeling and Multivariate Analysis

Table 5 provides regression output for various combinations of physical and flow properties, and provides predictive models for flowability parameters as functions of drying temperature and CDS levels. The ratio of Total Flow Index/Jenike Flow Function Index (-) yielded the highest R^2 (0.943), whereas the ratio of Total Flow Index/Total Flood Index (-) yields a slightly lower R^2 (0.920), but has the lowest standard error value (0.031). Thus, from a standard error point of view, Total Flow Index/Total Floodability Index = *f* (drying temperature, CDS levels) resulted in a better model for flowability than the Total Flow Index/Jenike Flow Function Index= *f* (drying temperature, CDS levels).

Both of these new response variables are dimensionless, and therefore yield versatile models for DDGS flowability. Additionally, these dimensionless parameters can overcome limitations imposed by the units. Techniques for combining two or more properties with similar units in order to achieve dimensionless parameters are often used in dimensional analysis and Exploratory Data Analysis (EDA) (21). Extensive work by others regarding flowability examined the dimensionless parameter ζ (equation 2), and obtained an R^2 value of about 0.92 (21). However, for our case, $R^2 = 0.64$ was obtained, as indicated in Table 5. Angle of repose ($R^2 = 0.88$) and Jenike Flow Function Index ($R^2 = 0.80$) yielded a better prediction of flowability than ζ. The Hausner Ratio, which is often used as a robust parameter to describe flowability, did not give promising results in this study, with $R^2 = 0.601$.

Response surface plots for AoR, HR, ζ, Jenike Flow Function, Total Flow Index/Jenike Flow Function, and Total Flow Index/Total Flood Index as functions of drying temperature and CDS levels are provided in Figures 7 through 12. For "good" flow behavior in DDGS, it was predicted that the ratio of Total Flow Index/Total Flood Index (-) should be from 1.25 to 1.29, which indicates that drying temperature should be >225°C and CDS < 14% (wb) or >17.5% (wb) (Figure 11). Perhaps higher CDS levels (>17.5%, wb) lubricates the material and produces better DDGS flow. Additionally, for "good" flow behavior in DDGS, it was predicted that the ratio of Total Flow Index/Jenike Flow Index (-) should be from 22.50 to 24.50, which means that the drying temperature should be between 200 to 260°C and CDS < 14% (wb) (Figure 12).

Another way to look at the data is by multivariate analysis. Figure 13a and Figure 13b represent the loading plot and model selection plot obtained from Partial Least Squares (PLS) regression for Jenike Flow Function Index as a function of all physical and flow variables, as listed in Table 1. Simple correlations between the original and the new variables are called the "loadings," and they indicate to what extent the original variables are influential in forming the new set of Principal Components. In other words, the higher the loading value of the variable, the more influential it is in forming the principal component scores.

Table 6 presents the summary results for the PLS regression modeling of Jenike Flow Index as a function of all other properties. It was observed that a high R^2 value of 0.90 using only 2 components was possible. Jenike Flow Index can easily be calculated from linear regression modeling whose coefficients are listed in Table 6. Therefore, the labor intensive task of the Jenike shear test procedure could be avoided.

From Figure 13a, for 2 components only, AoS, Compressibility, Total Flow Index, Hausner Ratio, and water activity were the variables which most influenced Jenike Flow Index. Figure 13b indicates $R^2 = 0.9$ using two principal components only, although 6 components resulted in an R^2 of nearly 0.97. Our experimental design had 26 dependent variables and 2 independent variables. PLS regression was found to be effective in reducing the multidimensional dataset to a fewer number of components without loss of information (45).

CONCLUSIONS

Based on our results, the flowability parameters such as Hausner Ratio, Jenike Flow Function, PDI, and ζ (a dimensionless flowability indicator) showed better flowability at higher drying temperatures. Also, at higher drying temperatures, fewer significant differences were observed in the flow and physical parameters among the CDS levels. Non-linear regression analyses developed with dimensionless flowability parameters resulted in $R^2 > 0.90$, and adequately represented the effects of CDS and drying temperature. Partial Least Squares (PLS) regression could effectively summarize the data with only two components, and provided a model for predicting Jenike Flow Index (-) as a function of all other flow and physical parameters. Thus, future flowability studies may be able to avoid performing the labor-intensive Jenike shear tests. Further studies with a larger sample size and more elaborate drying temperatures and CDS addition levels should be investigated. Additional studies to quantify flowability changes with varying cooling temperatures and times during storage should also be pursued in order to more fully understand DDGS flowability behavior.

ACKNOWLEDGEMENTS

The authors would like to extend their gratitude to South Dakota State University and USDA-ARS for financial support, equipment, and facilities for this project. We would like to thank Dakota Ethanol, LLC (Wentworth, SD) for contributing the coproduct samples for this study. The authors would also like to extend appreciation for financial support to the South Dakota Corn Utilization Council (SDCUC) and Agricultural Experimental Station (AES) as well.

REFERENCES

1. Chevanan, N.; Rosentrater K.A.; Muthukumarappan, K. Effect of DDGS, moisture content, and screw speed on physical properties of extrudates in single screw extrusion. Cereal Chemistry 2008, 85(2), 132-139.
2. AAFC: Protein meal: Situation and outlook. In Agriculture and Agri-Food Canada, Bi Weekly Bulletin, 2008; 19(3): 1-4. http://dsp-psd.pwgsc.gc.ca/Collection/A27-18-19-3E.pdf. Accessed on 14 October, 2011.
3. Bhadra, R.; Muthukumarappan, K.; Rosentrater, K.A. Flowability properties of commercial distillers dried grains with solubles. Cereal Chemistry 2009a, 86(2), 170-180.
4. Bhadra, R.; Rosentrater, K.A.; Muthukumarappan, K. Cross-sectional staining and surface properties of DDGS particles and their influence on the flowability. Cereal Chemistry 2009b, 86(4), 410-420.

5. Ganesan, V.; Rosentrater, K.A.; Muthukumarappan, K. Physical and flow properties of regular and reduced fat distillers dried grains with solubles (DDGS). Food and Bioprocess Technology 2007a, 2(2), 156-166.
6. Rock, M.; Schwedes, J. Investigations on the caking behaviour of bulk solids-macroscale experiments. Powder Technology 2005, 157(1-3), 121-127.
7. Cruz, C.R..; Brouk, M.J.; Schingoethe, D.J. Lactational response of cows fed condensed corn distillers solubles. Dairy Science 2005, 88(11), 4000-4006.
8. Rosentrater, K.A.; Muthukumarappan, K. Corn ethanol coproducts: generation, properties, and future prospects. International Sugar Journal 2006, 108(1295), 648-657.
9. Werner, S.L.R.; Fanshawe, R.L.; Paterson, A.H.J.; Jones, J.R.; Pearce, D.L. Stickiness of corn syrup powders by fluidized bed test. International Journal of Food Engineering 2006, 2(5), 1-10.
10. Ozkan, N.; Walisinghe, N.; Chen, X.D. Characterization of stickiness and cake formation in whole and skim milk powders. Food Engineering 2002, 55(4), 293-303.
11. Bronlund, J. Caking of spray dried lactose powders. PhD dissertation. Massey University; Auckland, New Zealand, 1996.
12. Shukla, P.R. Heat and mass transfer in packed food powders in relation to lumping and caking. Fourth Year Research Project; Department of Chemical and Materials Engineering. The University of Auckland; New Zealand, 2000. http://www.aiaa.org/agenda.cfm?lumeetingid=1188. Accessed on 14 October 2011.
13. Downton, G.E.; Flores-Lune, J.L.; King, C.J. Mechanism of stickiness in hydroscopic, amorphous powders. Industrial Engineering and Chemical Fundamentals 1982, 21(4), 447-451.
14. Wallack, D.A.; King, C., Sticking and agglomeration of hygroscopic, amorphous carbohydrate and food powders. Biotechnology Progress 1998, 4(1), 31-35.
15. Carr, R.L., Jr. Evaluating flow properties of solids. Chemical Engineering 1965, 72(3), 163-168.
16. Jenike, A.W. Storage and flow of solids. Bulletin No. 123. Utah Engineering Station; University of Utah; Salt Lake City, UT. 1964.
17. Michael, A.E. Pharmaceutics: The Science of Dosage Form Design (2nd edition); Churchill; Livingstone, UK, 2001.
18. Schulze, D. Storage of powders and bulk solids in silos, 2006. http://www.dietmer-schulze.de/storagepr.html. Accessed on 14 October, 2011.
19. Ganesan, V.; Muthukumarappan, K.; Rosentrater, K.A. Flow properties of DDGS with varying soluble and moisture contents using Jenike shear testing. Powder Technology 2008a, 187(2), 130-137.
20. Ganesan, V.; Muthukumarappan, K. Rosentrater, K.A. Effect of flow agent addition on the physical properties of DDGS with varying moisture content and soluble levels. Transactions of ASABE 2008b, 51(2), 591-601.

21. Ganesan, V.; Rosentrater, K.A.; Muthukumarappan, K. Modeling the flow properties of distillers dried grains with solubles (DDGS). Cereal Chemistry 2007b, 84(6), 556-562.

22. Ganesan, V.; Rosentrater K.A.; Muthukumarappan, K. Dynamic water adsorption characteristics of distillers dried grains with solubles. Cereal Chemistry 2007c, 84(6), 584-555.

23. Ganesan, V.; Muthukumarappan, K.; Rosentrater, K.A., Sorption isotherm characteristics of distillers dried grains with solubles (DDGS). Transactions of ASABE 2008c, 51(1), 169-176.

24. Bhadra, R.; Muthukumarappan, K.; Rosentrater, K.A. Physical and chemical characterization of fuel ethanol coproduct relevant to value-added uses. Cereal Chemistry 2010, 87(5), 439-447.

25. Bhadra, R.; Muthukumarappan, K.; Rosentrater, K.A.; Kannadhason, S. Drying characteristics of DWG with varying CDS and drying temperature levels. Applied Engineering in Agriculture 2009c, 27(5), 777-786.

26. Bhadra, R.; Rosentrater, K.A.; Muthukumarappan, K.; Kannadhason, S. Drying kinetics of DWG under varying CDS and temperature levels. Cereal Chemistry 2009d, 88(5), 451-458.

27. Rosentrater, K.A. Some physical properties of DDGS. Applied Engineering in Agriculture 2006, 22(4), 589-595.

28. ASTM: Method D6393 Standard test method for bulk solids characterization by Carr indices; American Society for Testing and Materials; West Conshohocken, PA.1999.

29. Mohsenin, N.N. Physical Properties of Plant and Animal Materials (2nd edition); Gordon and Breach Science Pub. Inc.; Amsterdam, Netherlands, 1986.

30. ASTM: Method D6128. Standard test method for shear testing of bulk solids using the Jenike Shear Cell; American Society for Testing and Materials; West Conshohocken, PA. 2006

31. ASTM: Method D6683 Standard test method for measuring bulk density values of powders and other bulk solids; American Society for Testing Materials; West Conshohocken, PA. 2001.

32. Baghe-Khandan, M.S.; Choi, Y.; Okos, M.R. Improved line heat source thermal conductivity probe. Food Science 1981, 46(5), 1430-1432.

33. ASAE: Standard S19.3 Method of determining and expressing fineness of feed materials by sieving; American Society of Agriculture Engineering Standards, Engineering Practices, Data; St Joseph, MI. 2003.

34. Sahin, S.; Sumnu, S.G. Physical Properties of Foods (1st edition); John Wiley and Sons; New York, NY, 1962.

35. AACC: Method 46-24. Protein dispersibility index; Approved Methods of American Association of Cereal Chemists, 10th edition; St Paul, MN. 1999.

36. Carmer, S.G.; Swanson, M.R.; An evaluation of ten pairwise multiple comparison procedures by Monte Carlo method. American Statistical Association 1973, 68(341), 66-74.

37. Speigel, M.R. Statistics (3rd edition); McGraw Hill, Inc.; New York, NY, 1994.

38. Grey, R.O.; Beddow, J.K. On Hausner Ratio and its relationship to some properties of metal powders. Powder Technology 1969, 2(6), 323-326.

39. Chegini, G.R.; Ghobadian, B. Spray dryer parameters for fruit juice drying. World Journal of Agricultural Science 2007, 3(2), 230-236.

40. Yan, H.; Barbosa-Canovas, G.V. Compression characteristics of agglomerated food powders. Effect of agglomerate size and water activity. Food Science and Technology International 1997, 3(5), 351-359.

41. Marinelli, J.; Carson, J.W. Solve solids flow problems in bins, hoppers, and feeders. Chemical Engineering Progress 1992, 88(5): 22-28.

42. Thomas, M.; Van Kol Edwin, M.R.A.H.; Tamminga, S.; Verstegen, M.W.A.; Van der Poel, A.F.B. Effect of water, steam and shear conditioning on the protein quality of soy grits. Science of Food and Agriculture 1997, 74(3), 392-400.

43. Qin, G.X.; Verstegen, M.W.A.; Van der Poel, A.F.B. Effect of temperature and time during steam treatment on the protein quality of full fat soybean from different origins. Science of Food and Agriculture 1998, 77(3), 393-398.

44. Chell, M. Properties and food applications of soy flours (T. H. Applewhite (ed): The American Oil Chemists Society). In Proceedings of World Conference on Oilseed Technology Utilization, Urbana, IL, September 13-18, 1992; 306-313.

45. Sharma, S. Applied Multivariate Techniques (1st edition); John Wiley and Sons; New York, NY, 1996.

46. Zhang, C. H; Huang, L. X; Wang, C. P.; Mujumdar, A. S. Experimental and numerical investigation of spray-drying parameters on the dried powder properties of ginkgo biloba seeds. Drying Technology 2010, 28(3), 380-388.

47. Kurozawa, L. E.; Morassi, A. G.; Vanzo, A. A.; Park, K. J.; Hubinger, M. D. Influence of spray drying conditions on physicochemical properties of chicken meat powder. Drying Technology, 2009, 27(11), 1248-1257.

48. Jiang, J.; Lu, J.; Huang, R.; Li, X. Effects of time and temperature on the viscoelastic properties of Chinese fir wood. Drying Technology, 2009, 27(11), 1229-1234.

49. Witrowa-Rajchert, D.; Rząca, M. Effect of drying method on the microstructure and physical properties of dried apples. Drying Technology, 2009, 27(7/8), 903-909.

Table 1: Main effects of drying temperature and CDS levels on resulting flow and physical properties of DDGS.*

	Temperature (°C)			CDS (% wb)		
Properties	**100**	**200**	**300**	**10**	**15**	**20**
Angle of Repose (°)	44.47b	44.86b	46.36a	42.86c	45.69b	47.12a
	(0.35)	(0.71)	(0.56)	(0.07)	(1.10)	(1.32)
Hausner Ratio (-)	1.17a	1.15a	1.09b	1.11b	1.14ab	1.15a
	(0.01)	(0.01)	(0.03)	(0.07)	(0.02)	(1.00)
Carr Compressibility (%)	14.71a	12.80a	7.88b	9.68b	12.17ab	13.54a
	(3.53)	(2.56)	(3.72)	(2.71)	(2.13)	(1.73)
Angle of Spatula (°)	53.95a	48.67c	49.26b	50.21c	50.96a	50.70b
	(1.07)	(1.10)	(0.97)	(1.21)	(1.32)	(1.10)
Uniformity (-)	2.26a	2.13b	1.86c	2.34a	2.05b	1.85c
	(0.13)	(0.01)	(0.01)	(0.11)	(0.20)	(0.01)
Total Flow Index (-)	75.86b	74.83b	79.40a	78.178a	75.25c	76.66b
	(3.15)	(1.06)	(1.26)	(2.17)	(1.64)	(1.72)
Angle of Fall (°)	41.27a	39.49a	38.90a	40.96a	41.00a	37.69b
	(2.17)	(1.93)	(2.00)	(1.94)	(1.16)	(1.15)
Angle of Difference (°)	3.19b	5.37ba	7.46a	1.89c	4.69b	9.43a
	(0.07)	(0.41)	(0.32)	(0.55)	(0.52)	(0.07)
Dispersibility (%)	39.30b	52.38a	47.88a	36.81c	64.07a	38.66b
	(5.32)	(4.73)	(4.62)	(4.84)	(3.70)	(3.62)
Total Flood Index (-)	63.83c	69.33a	67.17b	62.67c	69.83a	67.83b
	(1.32)	(1.26)	(2.17)	(2.07)	(3.15)	(3.02)
δ (°)	34.44a	36.22a	36.56a	39.00a	33.55b	34.66b
	(0.72)	(0.97)	(0.56)	(0.41)	(0.31)	(0.27)
Φ (°)	19.66b	24.79a	23.67a	24.22a	21.55a	22.33a
	(1.07)	(1.02)	(1.32)	(1.75)	(1.89)	(2.52)
σ_c (kPa)	21.57a	17.98b	18.98b	18.63b	20.33a	19.56a
	(0.65)	(0.57)	(0.41)	(0.72)	(0.81)	(0.32)
σ_1 (kPa)	40.21b	47.24a	36.87c	42.00a	42.54a	39.77b
	(2.13)	(2.13)	(1.72)	(1.42)	(1.37)	(1.26)
Jenike Flow Function Index (-)	1.87c	2.68a	2.18b	2.58a	2.09b	2.04b
	(0.11)	(0.02)	(0.31)	(0.25)	(0.71)	(0.81)
Jenike Compressibility (1/cm)	13.82ab	9.54b	16.30a	12.05ba	9.85b	17.76a
	(3.71)	(4.51)	(5.31)	(4.07)	(3.17)	(4.02)
Hunter L (-)	48.63a	46.43b	43.87c	45.51a	47.53b	45.89c
	(2.71)	(1.35)	(1.42)	(3.15)	(2.73)	(1.17)
Hunter a (-)	9.99a	10.05a	9.35b	9.74a	9.63a	10.01b
	(1.71)	(2.17)	(2.34)	(3.17)	(3.07)	(2.71)
Hunter b (-)	23.47a	21.93a	20.61c	21.91a	22.38b	21.69c
	(2.10)	(3.12)	(2.17)	(3.02)	(3.17)	(1.36)
a_w (-)	0.68a	0.44b	0.28c	0.40c	0.47b	0.52a
	(3.51)	(3.15)	(2.00)	(1.71)	(3.02)	(1.71)
Thermal Conductivity (W/((m)(°C))	0.06b	0.07a	0.07b	0.06b	0.06ab	0.07a
	(0.01)	(0.01)	(0.02)	(0.02)	(0.10)	(0.04)
Thermal Resistivity ((m)(°C)/W)	16.54a	15.06b	15.98a	17.12a	15.36b	15.08b
	(0.02)	(0.07)	(0.03)	(0.02)	(0.03)	(0.12)
Thermal Diffusivity (mm^2/s)	0.17a	0.15b	0.15b	0.17a	0.15b	0.15b
	(0.01)	(0.00)	(0.01)	(0.01)	(0.02)	(0.00)
Geometric Mean Diameter (mm)	0.73b	0.78b	0.99a	0.91a	0.75b	0.83ab
	(0.01)	(0.51)	(0.42)	(0.21)	(0.21)	(0.31)
Porosity (-)	0.58a	0.47b	0.47b	0.54a	0.51b	0.46c
	(2.13)	(3.17)	(1.51)	(2.17)	(2.07)	(1.91)
PDI (%)	9.3a	7.61b	7.21b	8.33a	7.59b	8.19a
	(2.11)	(1.45)	(3.02)	(0.89)	(1.02)	(1.50)

* Values with differing letters within a given row for a given independent variable are significantly different ($p<0.05$, LSD); values in parentheses indicate ±1 standard deviation; CDS is condensed distillers solubles (%, wb); δ is effective angle of internal friction (°); Φ is angle of internal friction (°) ; σ_c is unconfined yield strength (kPa); σ_1 is major consolidation stress (kPa); a_w is water activity (-); PDI is protein dispersibility index (%).

Table 2: Interaction effects (p-values) of drying temperature and CDS levels on resulting flow and physical properties of DDGS.*

Properties	Temperature (°C)	CDS (% wb)	CDS*Temp
Angle of Repose (°)	<0.0001	<0.0001	0.0003
Hausner Ratio (-)	0.0004	0.0344	0.2664
Carr Compressibility (%)	0.0003	0.033	0.2766
Angle of Spatula (°)	<0.0001	<0.0001	<0.0001
Uniformity (-)	<0.0001	<0.0001	<0.0001
Total Flow Index (-)	<0.0001	<0.0001	<0.0001
Angle of Fall (°)	<0.0001	<0.0001	<0.0001
Angle of Difference (°)	<0.0001	<0.0001	<0.0001
Dispersibility (%)	<0.0001	<0.0001	<0.0001
Total Flood Index (-)	<0.0001	<0.0001	<0.0001
δ (°)	0.0362	<0.0001	<0.0001
Φ (°)	0.0032	0.1519	0.0175
σ_c (kPa)	<0.0001	0.003	0.0042
σ_1 (kPa)	<0.0001	0.0002	<0.0001
Jenike Flow Function Index (-)	<0.0001	<0.0001	<0.0001
Jenike Compressibility (1/cm)	<0.0001	<0.0001	<0.0001
Hunter L (-)	<0.0001	<0.0001	<0.0001
Hunter a (-)	0.0012	0.1158	0.0019
Hunter b (-)	<0.0001	0.0871	0.0052
a_w (-)	<0.0001	<0.0001	<0.0001
Thermal Conductivity (W/((m)(°C))	0.0008	0.0221	0.0358
Thermal Resistivity ((m)(°C)/W)	<0.0001	<0.0001	<0.0001
Thermal Diffusivity (mm^2/s)	<0.0001	<0.0001	0.004
Geometric Mean Diameter (mm)	<0.0001	<0.0001	<0.0001
Porosity (-)	<0.0001	<0.0001	0.0176
PDI (%)	<0.0001	0.0006	0.0064

* Values in the table are the p-values determined by PROC GLM using SAS, $p<0.05$; CDS is condensed distillers solubles (%, wb); δ is effective angle of internal friction (°); Φ is angle of internal friction (°); σ_c is unconfined yield strength (kPa); σ_1 is major consolidation stress (kPa); a_w is water activity (-); PDI is protein dispersibility index (%).

Table 3: Treatment combination effects of drying temperature and CDS levels on resulting flow and physical properties of DDGS.*

	Temperature (°C)								
	100			200			300		
	CDS (% wb)			CDS (% wb)			CDS (% wb)		
Properties	10	15	20	10	15	20	10	15	20
Angle of Repose (°)	42.06c	44.71b	46.61a	42.02c	44.94b	47.62a	44.55c	47.43a	47.14b
	(0.42)	(0.61)	(0.51)	(0.31)	(0.25)	(0.75)	(0.44)	(0.37)	(0.31)
Hausner Ratio (-)	**1.13a**	**1.19a**	**1.20a**	**1.11a**	**1.15a**	**1.18a**	**1.09a**	**1.07a**	**1.09a**
	(0.02)	(0.07)	(0.00)	(1.17)	(1.21)	(0.05)	(1.03)	(1.71)	(1.21)
Carr Compressibility (%)	**11.28a**	**15.85a**	**17.00a**	9.39b	13.55ab	15.45a	**8.67a**	**7.120a**	**8.16a**
	(3.21)	(2.71)	(1.17)	(3.12)	(1.91)	(1.71)	(2.56)	(1.71)	(2.01)
Angle of Spatula (°)	55.86a	53.50b	52.49c	46.26c	50.18a	49.56b	48.51c	49.20b	50.05a
	(1.07)	(1.21)	(1.11)	(0.92)	(2.17)	(1.31)	(0.91)	(1.07)	(1.03)
Uniformity (-)	2.53a	2.00b	1.85c	2.51a	2.31a	1.95c	2.000a	1.840b	1.75c
	(0.01)	(0.21)	(0.01)	(0.31)	(0.02)	(0.01)	(0.03)	(0.21)	(0.01)
Total Flow Index (-)	77.83a	75.25b	74.50c	78.50a	74.50b	71.50c	**78.20a**	**79.00a**	**81.00a**
	(4.12)	(2.17)	(3.17)	(2.72)	(3.51)	(2.16)	(1.50)	(1.42)	(1.37)
Angle of Fall (°)	39.87c	40.75b	43.18a	**39.36a**	**39.750a**	**39.36a**	43.66a	42.50a	30.53b
	(1.41)	(1.37)	(1.21)	(1.06)	(1.21)	(1.03)	(0.04)	(0.51)	(0.72)
Angle of Difference (°)	2.19b	3.96a	3.43ab	2.66c	5.193b	8.26a	0.84c	4.93b	16.60a
	(0.07)	(0.09)	(1.02)	(0.06)	(1.21)	(1.03)	(0.04)	(0.51)	(0.72)
Dispersibility (%)	41.70b	46.07a	30.13c	34.16c	73.40a	49.57b	34.59b	72.75a	36.29b
	(3.71)	(4.02)	(5.72)	(4.62)	(3.12)	(2.17)	(5.07)	(4.31)	(3.76)
Total Flood Index (-)	61.00b	70.00a	60.50c	65.50c	70.00b	72.50a	61.50c	69.50b	70.50a
	(1.71)	(2.07)	(1.51)	(1.32)	(1.40)	(0.91)	(2.16)	(1.73)	(1.51)
δ (°)	37.66a	33.33b	32.33b	34.33b	35.33b	39.00a	45.00a	32.00b	32.66b
	(0.45)	(0.32)	(0.21)	(0.74)	(0.51)	(0.71)	(0.64)	(0.81)	(1.02)
Φ (°)	17.33b	21.66a	20.00ab	27.00a	22.33b	25.00a	**28.33a**	**20.66a**	**22.00a**
	(1.01)	(1.07)	(1.21)	(1.31)	(0.75)	(0.51)	(1.72)	(2.01)	(2.31)
σ_c (kPa)	21.94a	21.68a	21.09a	15.67b	19.93a	18.32a	**18.27a**	**19.39a**	**19.28a**
	(0.41)	(0.21)	(0.23)	(0.71)	(0.50)	(1.51)	(1.72)	(1.63)	(1.54)
σ_1 (kPa)	37.68b	42.13a	40.81a	53.22a	45.91b	42.59c	35.11b	39.58a	35.91b
	(1.71)	(1.52)	(1.31)	(0.72)	(0.56)	(1.15)	(1.72)	(1.63)	(1.54)
Jenike Flow Function Index (-)	1.72b	1.94a	1.94a	3.39a	2.30b	2.33b	2.64a	2.03b	1.86c
	(0.11)	(0.02)	(0.00)	(0.31)	(0.71)	(0.31)	(0.43)	(0.500	(0.37)
Jenike Compressibility (1/cm)	12.57b	7.10c	21.79a	2.19b	12.82a	13.61a	21.39a	9.64c	17.87b
	(4.12)	(3.17)	(2.71)	(5.16)	(5.01)	(3.74)	(3.02)	(1.21)	(1.94)
Hunter L (-)	46.22c	51.72a	47.94b	**47.24a**	**46.67a**	**45.38a**	43.07b	44.18a	44.36a
	(2.17)	(1.23)	(2.13)	(1.93)	(1.16)	(1.53)	(1.62)	(2.10)	(0.77)
Hunter a (-)	9.48b	9.80ba	10.68a	10.59a	9.51b	10.03ba	**9.13a**	**9.59a**	**9.32a**
	(2.01)	(1.71)	(1.51)	(1.010	(0.09)	(0.91)	(0.72)	(0.77)	(0.73)
Hunter b (-)	22.94ab	24.73a	22.73b	22.66a	21.68ab	21.45b	20.15b	20.75a	20.91a
	(2.13)	(1.71)	(1.63)	(1.63)	(2.07)	(0.17)	(0.89)	(1.31)	(0.74)
a_w (-)	0.64c	0.68b	0.71a	0.33c	0.46b	0.54a	0.23c	0.28b	0.32a
	(0.71)	(0.43)	(0.06)	(0.31)	(0.21)	(0.01)	(1.20)	(1.03)	(0.17)
Thermal Conductivity (W/((m)(°C))	0.06b	0.06b	0.07a	**0.07a**	**0.07a**	**0.07a**	**0.06a**	**0.07a**	**0.066a**
	(0.03)	(0.31)	(0.01)	(0.02)	(0.04)	(0.05)	(0.03)	(0.01)	(0.00)
Thermal Resistivity ((m)(°C)/W)	17.86a	16.73b	15.03c	15.30a	14.60b	15.26a	18.20a	14.76b	14.96b
	(0.01)	(0.01)	(0.07)	(0.06)	(0.64)	(0.05)	(0.04)	(0.06)	(0.51)
Thermal Diffusivity (mm^2/s)	0.18a	0.173a	0.16b	0.16a	0.143a	0.15a	0.17a	0.14b	0.14b
	(0.01)	(0.34)	(0.07)	(0.06)	(0.17)	(0.12)	(0.51)	(0.42)	(0.31)
Geometric Mean Diameter (mm)	0.69b	0.67c	0.82a	0.72c	0.79b	0.83a	1.31a	0.81c	0.85b
	(0.13)	(0.71)	(0.53)	(0.07)	(0.06)	(0.51)	(0.41)	(0.31)	(0.27)
Porosity (-)	0.61a	0.57b	0.55b	0.49a	0.49a	0.43b	0.53a	0.47b	0.42c
	(1.37)	(2.01)	(3.14)	(1.42)	(2.15)	(2.14)	(1.71)	(1.62)	1.06)
PDI (%)	**9.56a**	**9.34a**	**8.98a**	8.10a	6.85b	7.88a	7.33a	6.59ab	7.71a
	(0.71)	(1.45)	(3.51)	(1.03)	(3.12)	(4.02)	(3.140	(0.89)	(0.93)

* Values with differing letters within a given row are significantly different ($p<0.05$, LSD) across all treatment combinations; values in parentheses indicate ±1 standard deviation; bold numbers indicate values for which there were no significant differences amongst the CDS levels for a given drying temperature level. CDS is condensed distillers solubles (%, wb); δ is effective angle of internal friction (°); Φ is angle of internal friction (°); σ_c is unconfined yield strength (kPa); σ_1 is major consolidation stress (kPa); a_w is water activity (-); PDI is protein dispersibility index (%).

Table 4: Pearson linear correlation coefficients (r) between resulting flow and physical properties for DDGS prepared using varying drying temperature and CDS combinations. Only significant (p< 0.05) correlations are listed*

Variable combinations	r	p-value
Thermal Conductivity × Temperature	-0.936	<0.0001
Angle of Difference × Angle of Fall	-0.889	<0.0001
Angle of Repose × Uniformity	-0.881	<0.0001
σ_1 × Jenike Compressibility	-0.857	<0.0001
Temperature × a_w	-0.820	<0.0001
Jenike Compressibility × Angle of Spatula	-0.796	<0.0001
Temperature × Hunter a	-0.792	<0.0001
CDS × Uniformity	-0.736	<0.0001
Thermal Diffusivity × Thermal Resistivity	-0.716	<0.0001
Temperature × Angle of Spatula	-0.705	<0.0001
Thermal Conductivity × Carr Compressibility	0.705	<0.0001
Thermal Conductivity × Hunter a	0.721	<0.0001
a_w × Thermal Conductivity	0.736	<0.0001
PDI × Geometric Mean Diameter	0.743	<0.0001
Thermal Conductivity × Angle of Spatula	0.796	<0.0001
Thermal Diffusivity × Geometric Mean Diameter	0.828	<0.0001
Hunter a × a_w	0.852	<0.0001
σ_1 × Angle of Spatula	0.867	<0.0001
Hausner Ratio × Carr Compressibility	0.998	<0.0001

* CDS is condensed distillers solubles level (%, wb); σ_1 is major consolidation stress (kPa); a_w is water activity (-); PDI is protein dispersibility index (%).

Table 5: Prediction models for selected dependent variables developed by response surface regression.*

Dependent Variable	z	AOR (-)	HR (-)	Jenike Flow Function Index (-)	ζ (-)	Total Flow Index/Total Flood Index (-)	Total Flow Index/Jenike Flow Function Index (-)
	x	Temperature	Temperature	Temperature	Temperature	Temperature	Temperature
Independent Variable	y	CDS	CDS	CDS	CDS	CDS	CDS
Prediction Equation		$z=a+bx^3+c/y$	$z^{-1}=a+bx^3+c/y$	$z^{-1}=a+b/\ln x+c/x^{0.5}+d\ln y+e/\ln y$	$z=a+b/x+cy^3$	$z=(a+bx+cx^2+d\ln y)/(1+ex+fx^2+g\ln y+h(\ln y)^2)$	$z=a+b\ln x+c/y+d(\ln x)^2+e/y^2+f(\ln x)/y$
Model Performance	R^2	0.881	0.601	0.804	0.643	0.920	0.943
	Adjusted R^2	0.865	0.549	0.757	0.596	0.884	0.926
	F statistic	88.733	18.091	22.512	21.610	31.096	69.793
	Standard error	0.760	0.037	0.242	0.142	0.031	1.858
Model Parameters	a	5.05E+01	7.89E-01	2.60E+01	-9.37E-03	-9.73E-01	8.38E+02
	b	7.39E-08	2.63E-09	-1.77E+02	5.85E+01	-2.98E-03	-3.36E+02
	c	-8.52E+01	8.08E-01	1.76E+02	2.44E-05	6.17E-06	1.92E+03
	d			-8.16E-01		3.76E-01	3.51E+01
	e			-6.77E+00		-3.44E-03	1.08E+02
	f					7.53E-06	-3.93E+02
	g					-9.81E-01	
	h					2.38E-01	
Figure No.		7	8	9	10	11	12

* AoR is angle of repose (°); HR is Hausner Ratio (-); CDS is condensed distillers solubles level (% wb); ζ is an empirical flowability indicator defined as = (C_c/Dispersibility)*(δ/Φ) (Ganesan et al., 2007b). Each equation is plotted in the denoted figure.

Table 6. Partial Least Squares (PLS) regression results for Jenike Flow Function Index (-) as a multivariate function of all other flow and physical properties (excluding the Jenike properties).

Predictor Variables	Parameter Estimates
Constant	9.6106
Angle of Repose	-0.0817
Hausner Ratio	0.2675
Compressibility	0.0036
Angle of Spatula	-0.1203
Uniformity	0.2858
Total Flow Index	-0.0100
Angle of Fall	0.0145
Angle of Difference	-0.0272
Dispersibility	-0.0115
Total Flood Index	0.0301
Water Activity	-0.2967
Thermal Conductivity	12.4430
Thermal Diffusivity	-0.9390
Geometric Mean Diameter	0.0266
Porosity	-0.4575
R^2	0.90
p-Value	0.0001
F Statistic	100.39
PLS Components Required	2

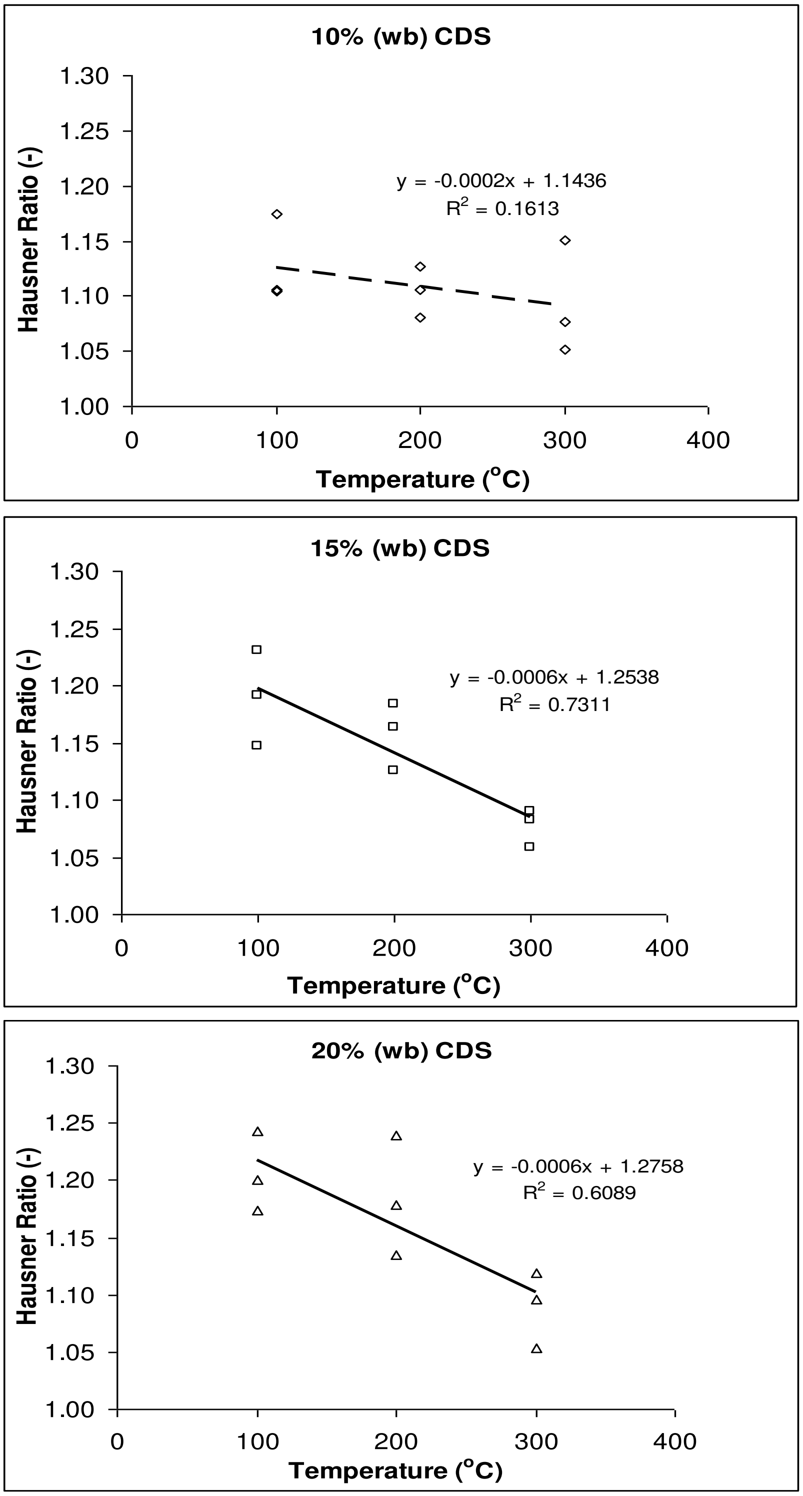

Figure 1: Relationships between Hausner Ratio and drying temperature according to CDS level.

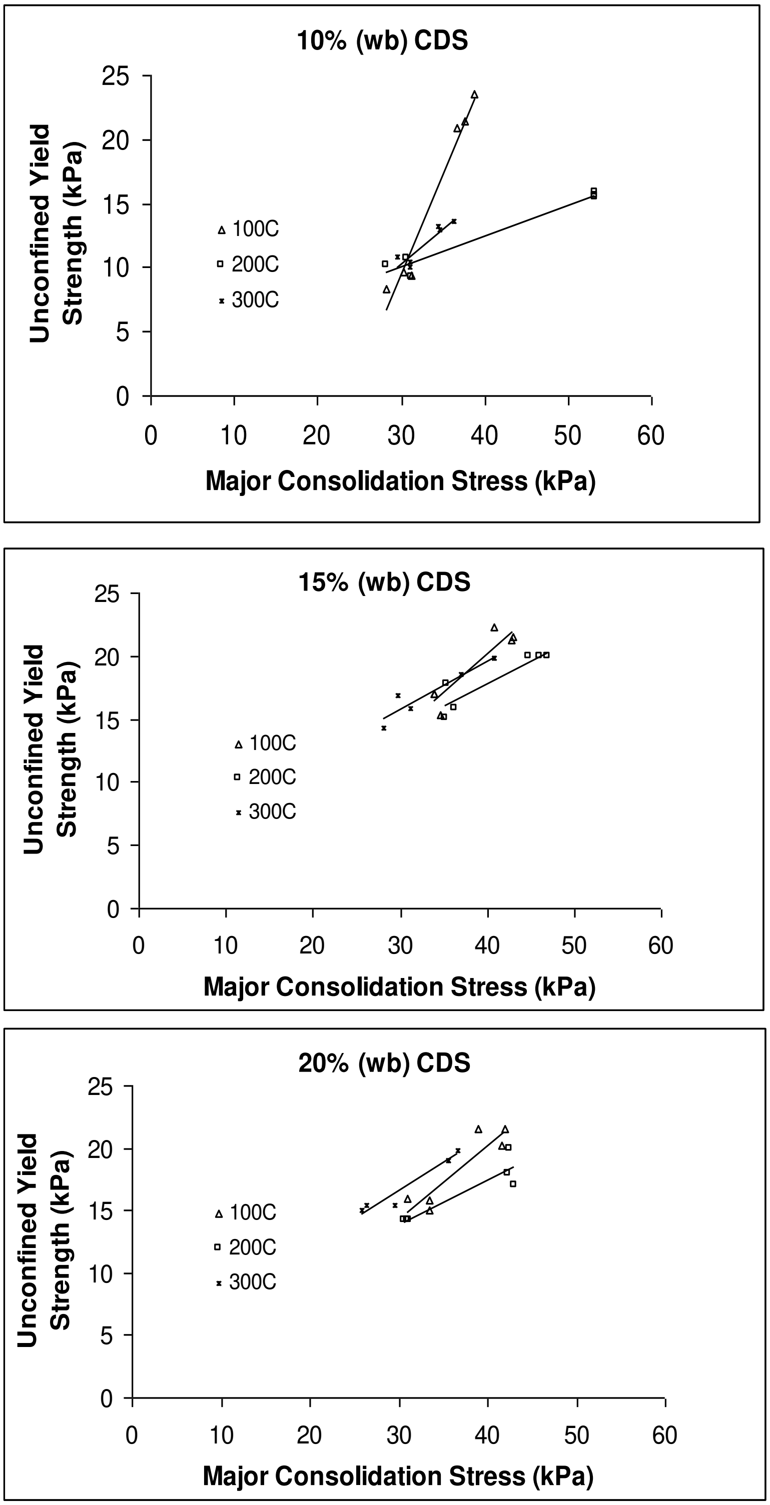

Figure 2: Relationships between unconfined yield strength (σ_c), major consolidation stress (σ_1), (which are known as Jenike Flow Function curves), and drying temperature according to CDS level.

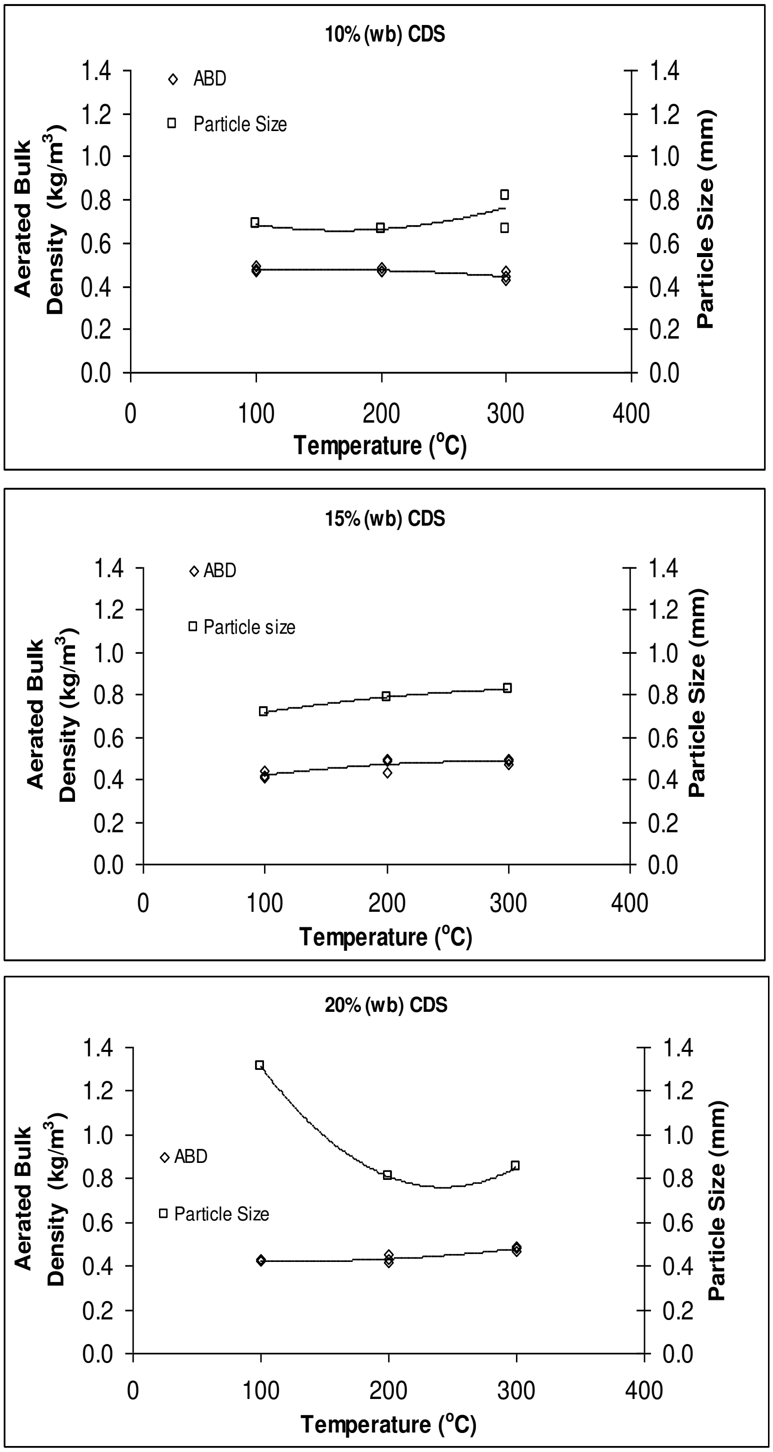

Figure 3: Relationships between aerated bulk density (ABD), particle size, and drying temperature according to CDS level. Particle size is defined as geometric mean diameter (d_{gw}).

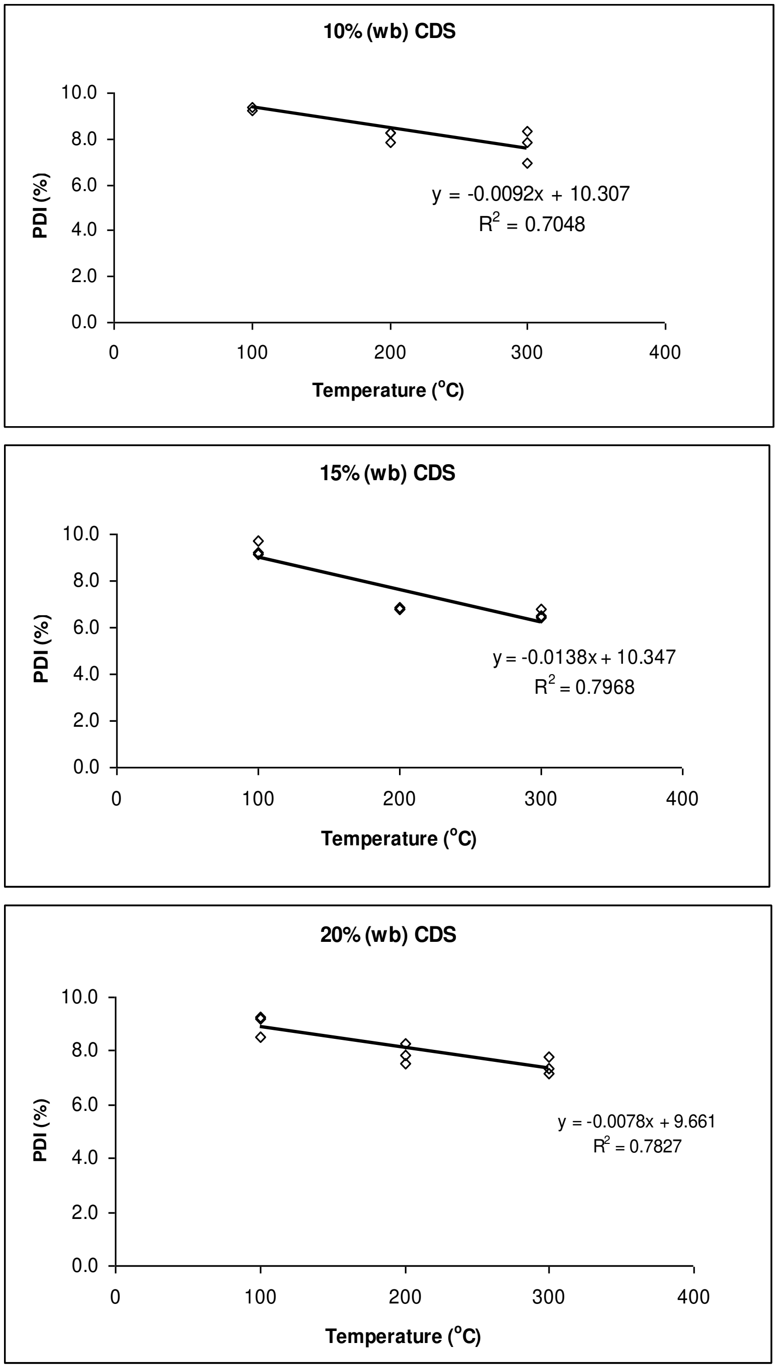

Figure 4: Relationships between protein dispersibility index (PDI) and drying temperature according to CDS level.

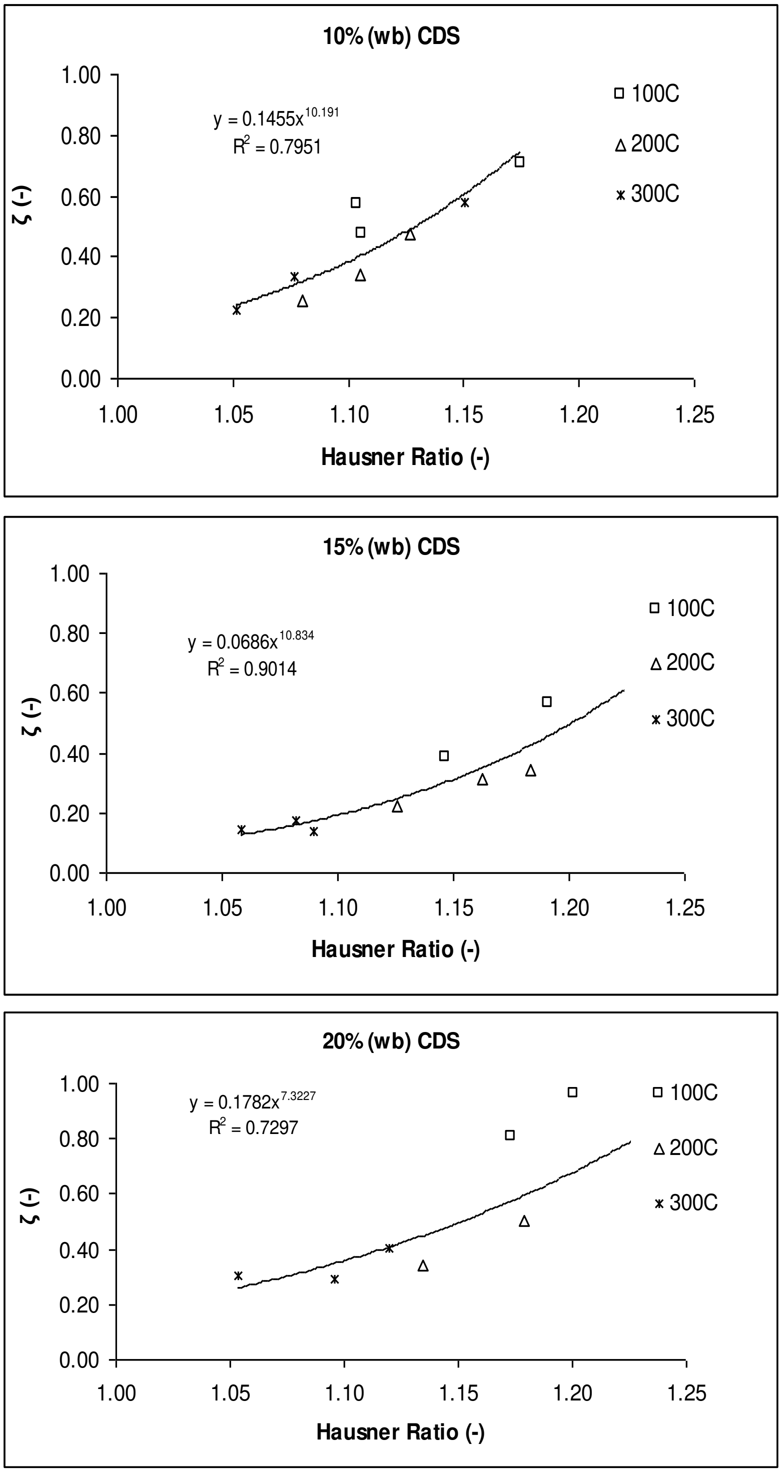

Figure 5: Validation of empirical flowability model (from Ganesan et al., 2007b) by fitting power law regression equations according to CDS level; ζ is defined as (C_c/Dispersibility)*(δ/Φ).

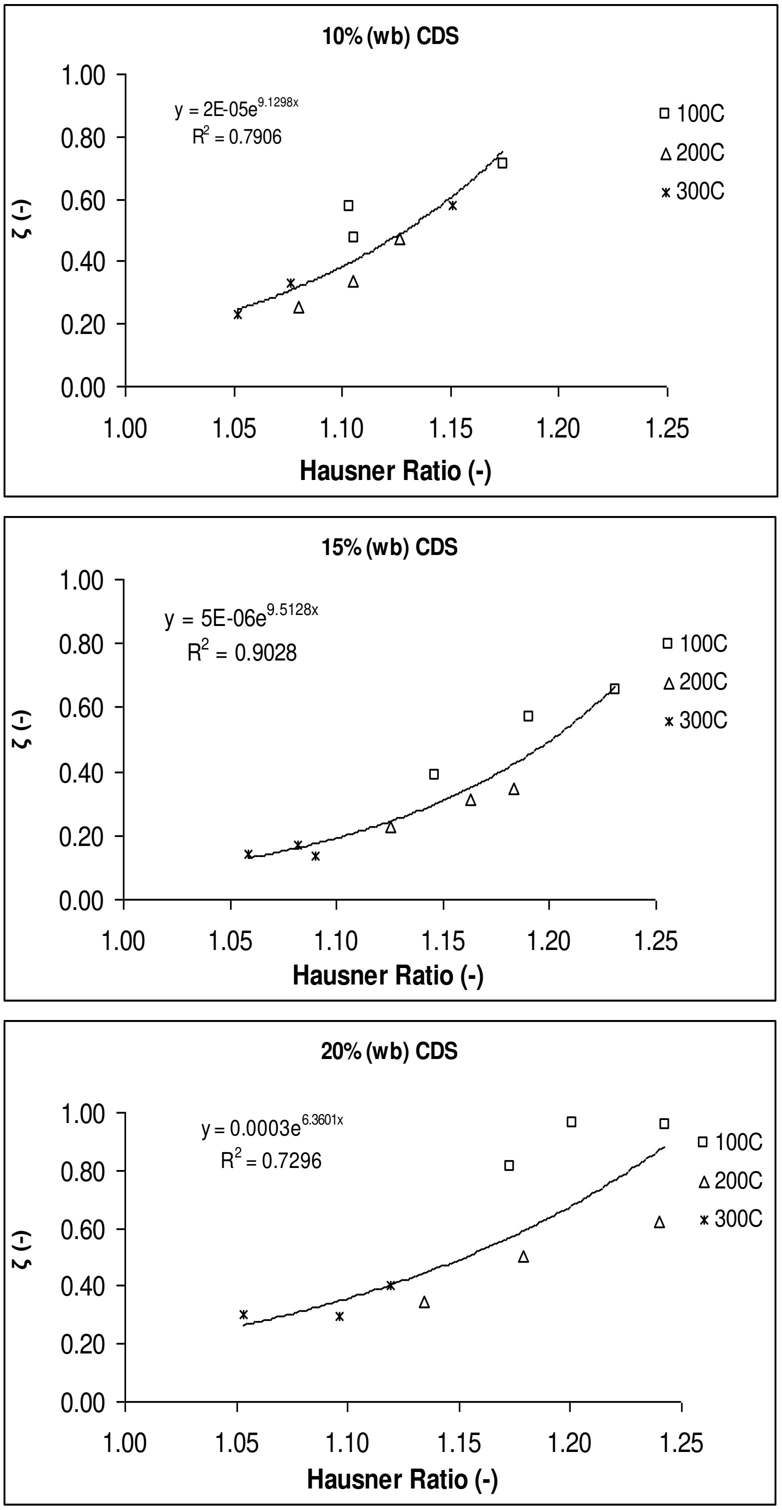

Figure 6: Validation of empirical flowability model (from Ganesan et al., 2007b) by fitting exponential regression equation, according to CDS level; ζ is defined as (C_c/Dispersibility)*(δ/Φ).

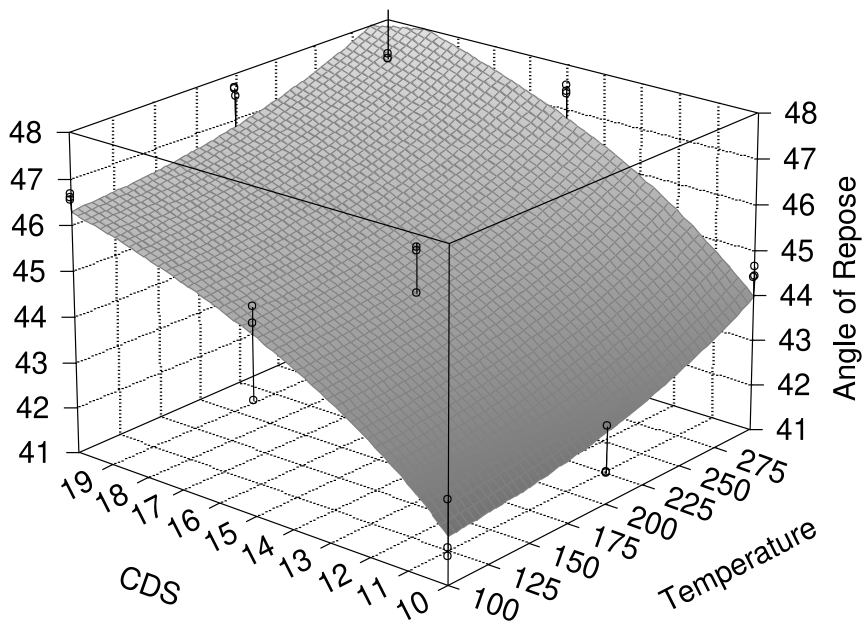

Figure 7: Surface plot showing the relationship between drying temperature (°C), CDS level (% wb), and angle of repose (°).

661

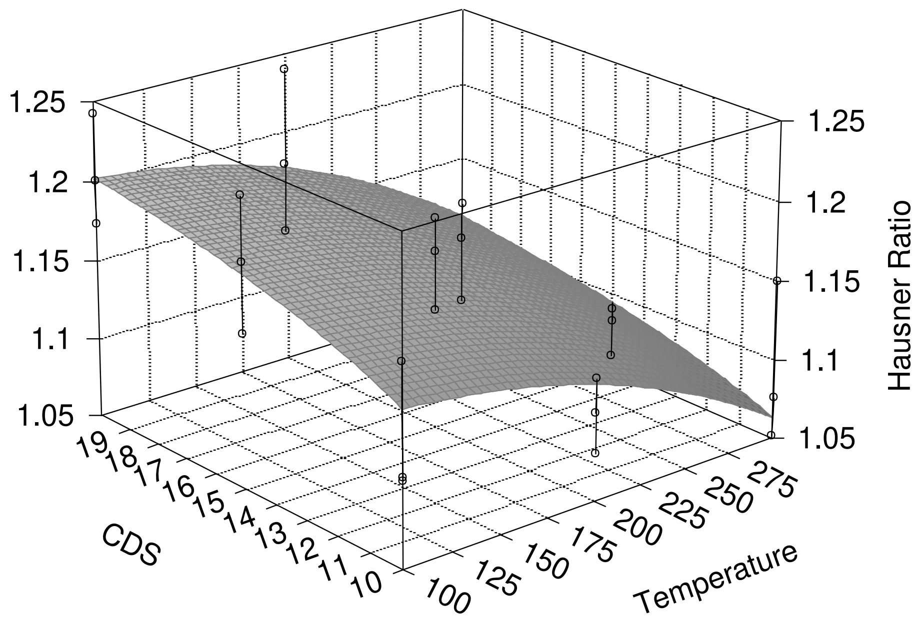

Figure 8: Surface plot showing the relationship between drying temperature (°C), CDS level (% wb), and Hausner Ratio (-).

662

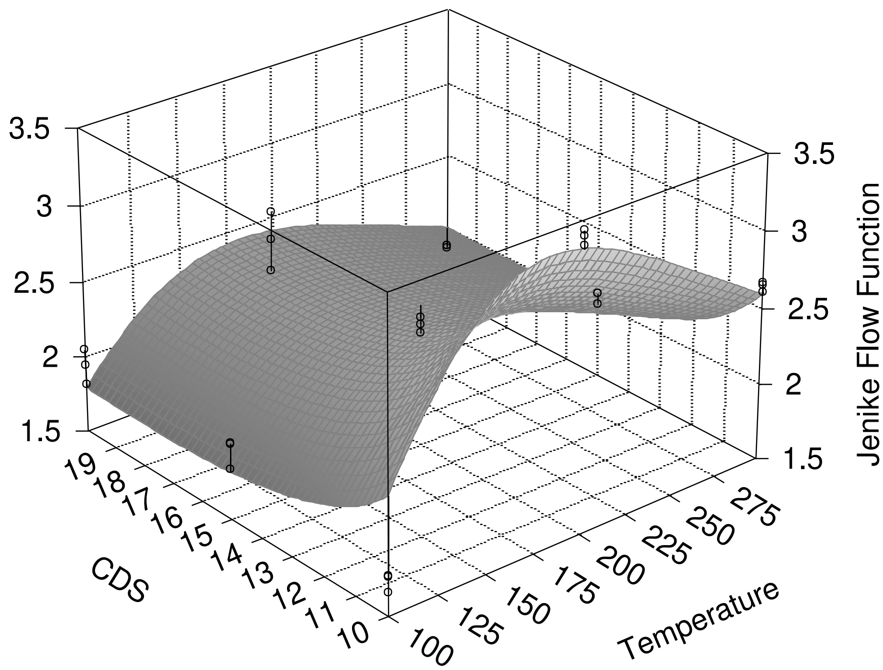

Figure 9: Surface plot showing the relationship between drying temperature (°C), CDS level (% wb), and Jenike Flow Function Index (-) [note that Jenike Flow Function Index is also known as Jenike Flow Index (-)].

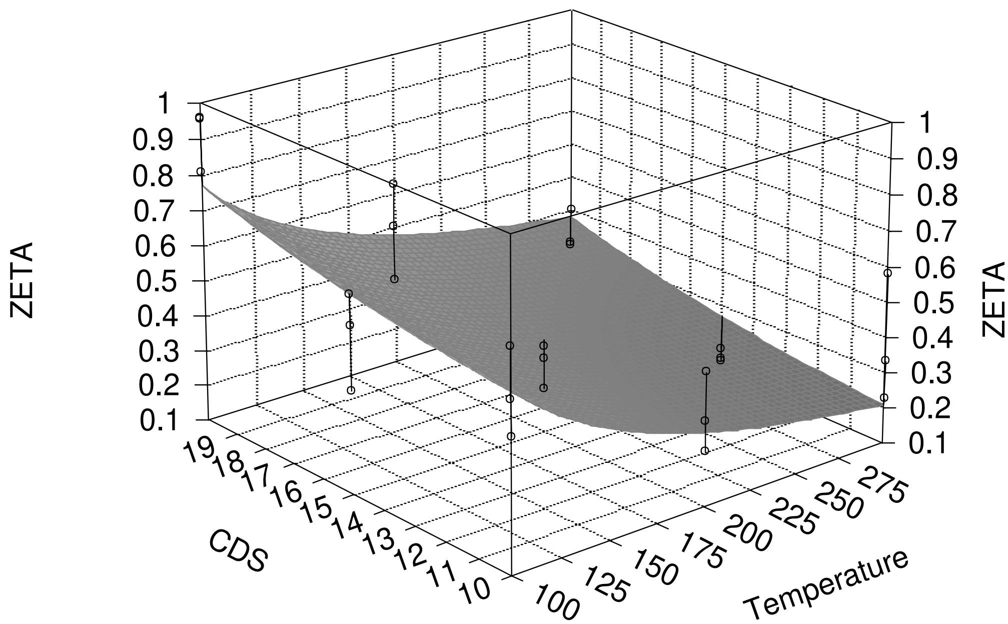

Figure 10: Surface plot showing the relationship between drying temperature (°C), CDS level (% wb), and zeta (ζ, -). Zeta is the empirical flowability indicator.

664

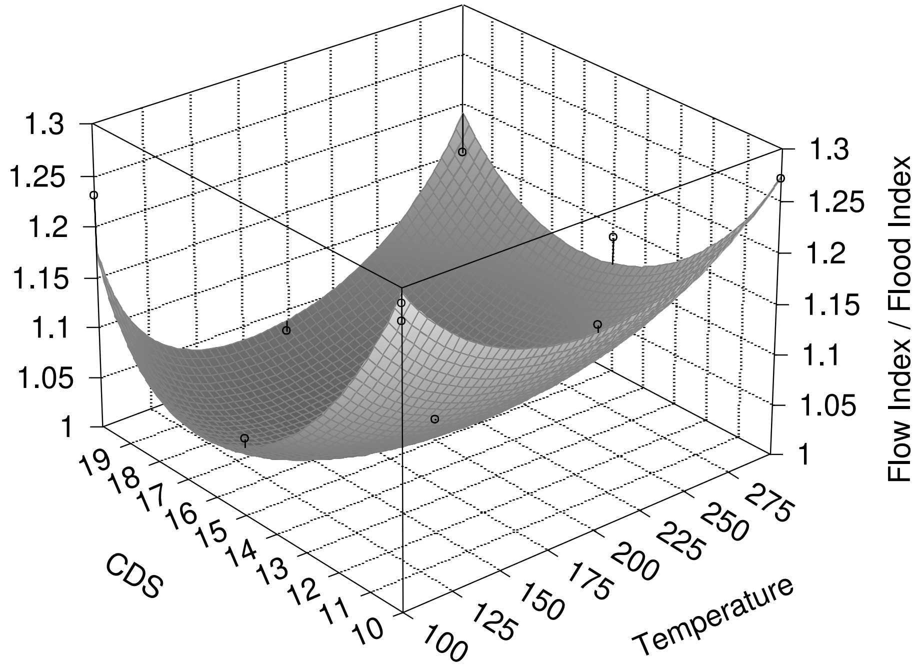

Figure 11: Surface plot showing the relationship between drying temperature (°C), CDS level (% wb), and the ratio of Total Flow Index/Total Flood Index.

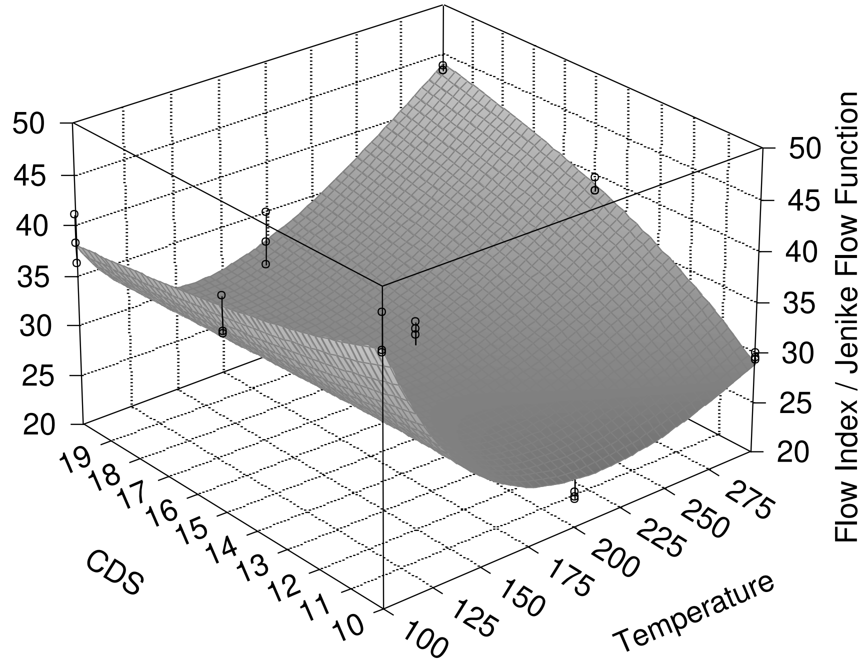

Figure 12: Surface plot showing the relationship between drying temperature (°C), CDS level (% wb), and the ratio of Total Flow Index/Jenike Flow Function Index [note that Jenike Flow Function Index is also known as Jenike Flow Index (-)].

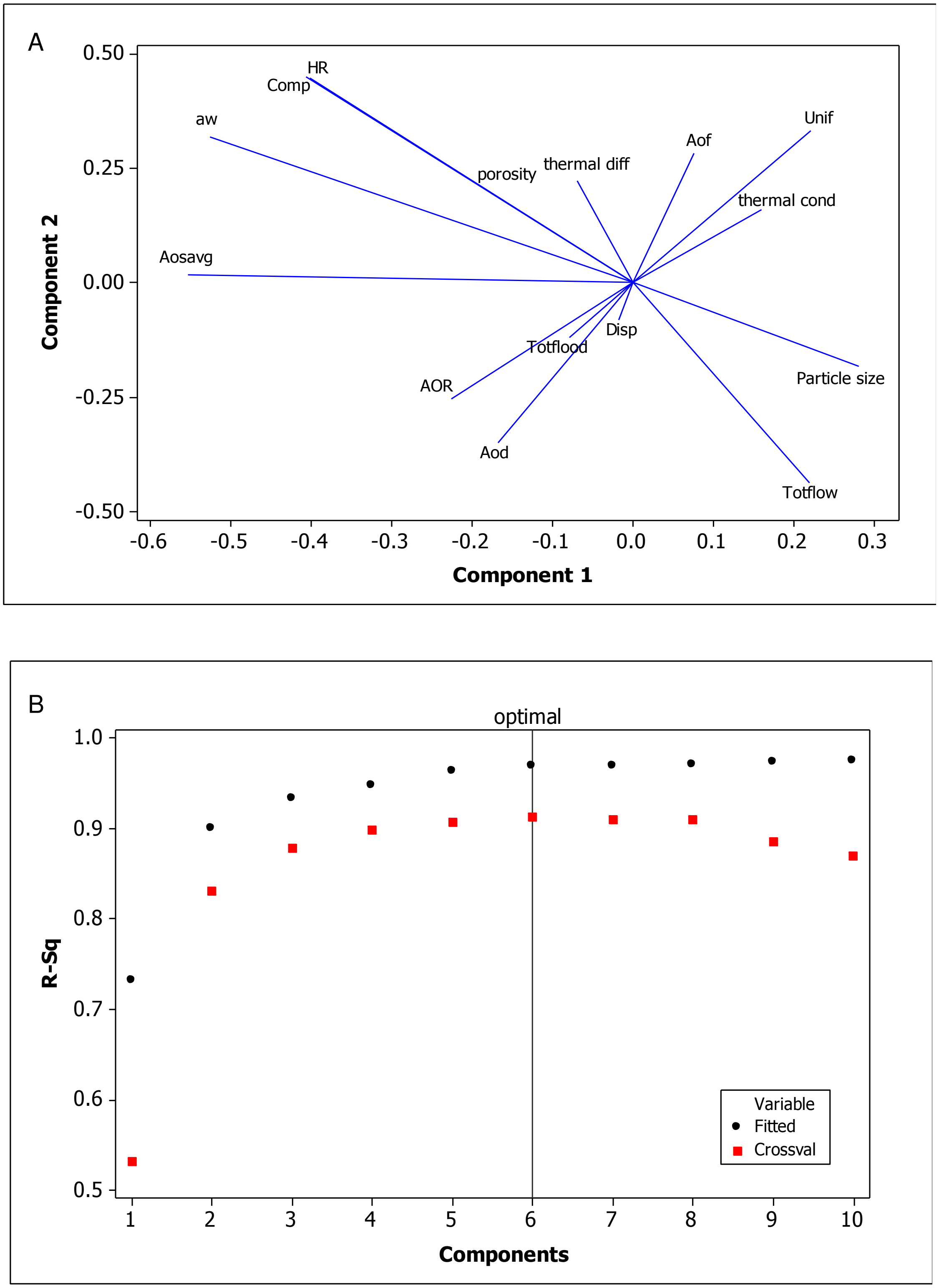

Figure 13. Partial Least Square (PLS) regression results for Jenike Flow Function Index as a multivariate function of all flow and physical properties (excluding Jenike properties); (A) loading plot; (B) model selection plot for the PLS analysis. [“R-sq” is the coefficient of determination (R^2); “Fitted” indicates the fitted PLS regression line; “Cross val” is cross validation, which is a

multivariate procedure used to predict and validate the PLS regression curve by using alternative data points from the entire data set and testing the line fit].